4D Printed Biocompatible Magnetic Composite for Minimally Invasive Deployable Structures

Saswat Choudhury[1], Akshat Joshi[1], Debayan Dasgupta[2], Ambarish Ghosh[2,3], Sonal Asthana[4,5], Kaushik Chatterjee[1,4#]

[1]Centre for BioSystems Science and Engineering, Indian Institute of Science, C.V. Raman Avenue, Bangalore, India 560012

[2]Centre for Nanoscience and Engineering, Indian Institute of Science, C.V. Raman Avenue, Bangalore, India 560012

[3]Department of Physics, Indian Institute of Science, C.V. Raman Avenue, Bangalore, India 560012

[4]Department of Materials Engineering, Indian Institute of Science, C.V. Raman Avenue, Bangalore, India 560012

[5]Department of Hepatobiliary and Multi-Organ Transplantation Surgery, Aster CMI Hospital, Bangalore, India 560024

#Corresponding author:

kchatterje@iisc.ac.in; +91-80-22933408

Abstract

4D printing of shape memory polymers (SMPs) and composites has been realized for a multitude of applications spanning healthcare, soft robotics, environment, space, etc. However, demonstrating such materials for *in vivo* applications has not been possible to a large extent due to the unavailability of suitable materials with recovery temperatures around physiological levels. Also, direct heating to trigger shape recovery in SMPs is not a practical and elegant approach in many cases. In this study, polylactide-co-trimethylene carbonate (PLMC), an SMP, has been endowed with magnetic iron oxide (Fe_3O_4) nanoparticles to realize remote heating under alternating magnetic field and at temperatures around 40°C. The PLMC-5% Fe_3O_4 composite was 3D printed into a variety of shapes, including scaffolds, fixed into pre-programmed temporary shapes to be deployed minimally invasively, and then recovered into original shapes under magnetic actuation. The shape recovery was excellent (>99%) and fast (under 20-30 s). Additionally, these magnetic composites could potentially be guided to the site of deployment through permanent magnets. Both PLMC and its composites were printed in distinct regions of a single structure, deformed, and then recovered by selective and sequential stimulation of magnetic field and heat, respectively. The materials (both PLMC and its nanocomposite) exhibited favorable *in vitro* and *in vivo* biocompatibility, thus highlighting their usefulness for being used as deployable tissue scaffolds and medical devices, among other implantable applications.

Keywords: shape memory polymers; biomaterials; minimally invasive surgery; smart materials; nanocomposites

1. Introduction

The field of additive manufacturing has advanced rapidly and is increasingly being adapted to meet the challenging demands of various sectors, including environment[1], robotics[2], healthcare[3], etc. Four-dimensional (4D) printing is the latest addition to this fascinating field. It combines three-dimensional (3D) printing with smart materials. Smart materials used are typically shape-memory polymers (SMPs), which exhibit the unique property of stabilizing a temporary deformed shape and subsequent recovery back to their original shape by the application of an external stimulus[4]. This property stems from the distinct molecular architectures of the polymers. The presence of such distinct phases in the polymer allows it to be fixed into a temporary shape by deformation (governed by netpoints or hard segments) below the transition temperature, followed by recovery into original shape (influenced by molecular switches or soft segments) upon heating it above the transition temperature. Owing to this intrinsic property of temperature-assisted shape recovery, SMPs have been explored for various potential applications, such as soft robotics[5], grippers[6], self-deployable structures in space applications[7], and biomedical applications[8].

In the field of biomedicine, it is also essential that the SMP being used is biocompatible and preferably biodegradable. There exists only a handful of polymer candidates meeting these stringent requirements, such as polylactic acid[9] (PLA), polyurethanes[10] (PUs), their blends, epoxy-based thermosets[11], etc. However, these materials are associated with serious drawbacks such as difficult processability, minimal recovery performance, high recovery temperatures, which limits their applicability *in vivo*, etc. SMPs could be useful for facilitating minimally invasive procedures, wherein the fixed and compressed shape can be deployed at the target site, and the SMP can then recover to its original shape upon specific stimulation. SMPs have been proposed for cardiovascular stents[12], clot removal devices[13], self-tightening wound closure

devices[14], etc. When the stimulus used is light, the shape memory function can be combined with laser treatment for photodynamic therapy for cancer[15].

Polylactide-co-trimethylene carbonate (PLMC), a biodegradable polymer, has been explored as a versatile shape memory polymer in some studies for biomedical applications[16]. The distinct advantage is its glass transition temperature (T_g), which lies close to the physiological temperature, rendering it a promising candidate for *in vivo* applications. However, triggering shape recovery through direct heating is not feasible in many cases, particularly for *in vivo* applications requiring intraoperative stimulation. Owing to poor thermal conductivity of the polymers, the entire surrounding region must be heated up, which could take a long time and the shape change may not be uniform. Thus, athermal heating, which is possible by careful selection of the nanofillers incorporated in the polymer matrix, is a potentially viable means of exploiting the shape memory materials for remote actuation. The stimulus could be light[17], ultrasound[18], water[19], microwaves[20], etc. Magnetic stimulation is a potential means of remote actuation of these materials via indirect heating. The most popular nanofiller in this regard is iron oxide (Fe_3O_4) nanoparticles which have an excellent inductive heating ability. Fe_3O_4 nanoparticles have far-reaching applications in biomedicine, including hyperthermia for cancer treatment[21], magnetic resonance imaging contrast agents[22], etc. These nanoparticles also have the ability to transfer energy from the radio-frequency field to surrounding media via heat dissipation[23]. However, utilizing Fe_3O_4 nanoparticles to activate recovery of SMPs is barely explored. So far, one study has reported the incorporation of Fe_3O_4 in PLA and crosslinked PLA matrices to yield composites and demonstrated the shape recovery of the composites inside alternate magnetic field[24]. However, the drawback of this material is its high recovery temperatures (70°C), complex chemical modifications to crosslink PLA, difficult processability involving solvents, high filler concentrations, etc. The other few studies based

on PLA and Fe_3O_4 composites[25-26] are also not devoid of the mentioned drawbacks which limit their applications *in vivo* as deployable scaffolds.

In this work, PLMC as an SMP has been endowed with Fe_3O_4 nanoparticles to realize remote actuation through a magnetic field. PLMC- 5% Fe_3O_4 composites were 3D printed via extrusion-based technology into simple two-dimensional (2D) shapes and 3D shapes, including tissue scaffolds (as shown in figure 1). Extrusion printing is advantageous over other modalities like direct ink writing, which requires tedious optimization and longer times for complete removal of solvent from the printed structures[27], etc. The composites were athermally triggered under an alternating magnetic field, highlighting free as well as restrictive shape memory properties. Dual material printing was also performed to spatially lay down PLMC and its composite in specific parts of the same structure. The dual-printed structures were selectively and sequentially actuated through inductive and direct heating. The materials were tested for thermal properties, shape memory properties, and finally, biological response *in vitro* and *in vivo*.

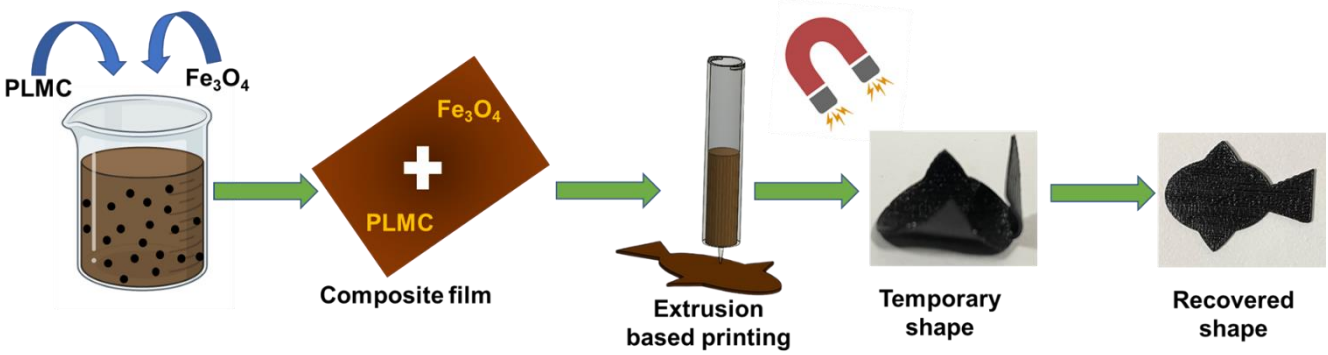

Figure 1: Schematic of the composite preparation and 3D printing followed by magnetic actuation for shape recovery

2. Experimental

2.1 Materials

PLMC was purchased from Evonik Ltd, Germany. Magnetite nanoparticles (of size range 50-100 nm) were purchased from Sigma Aldrich Pvt Ltd. Dichloromethane (DCM) of analytical grade was purchased from Sigma Aldrich.

2.2 Fabrication and 3D printing of PLMC-Fe_3O_4 nanocomposites

PLMC was dissolved in DCM (0.15 g/mL) under continuous magnetic stirring till a clear homogeneous solution was obtained. Fe_3O_4 nanoparticles were sonicated in DCM using probe sonication for about 40 min till a well-dispersed suspension was obtained. The suspension was then transferred into the polymer solution, and the resulting solution was further bath sonicated for another 40 min for the particles to homogeneously disperse in the polymer matrix. This solution was then cast over Teflon sheets and left to dry overnight. The composite film, obtained upon drying of the solvent, was then kept inside a vacuum oven for about 48 h to completely remove any traces of solvent present in the film. The obtained film was chopped into smaller pieces and fed inside the metal cartridge of the 3D printer (BioX, CELLINK).

Printing parameters were optimized to get good accuracy and resolution of the composite structures. Printing temperatures were in the range of 200°C to 210°C, the pressure of about 200 MPa, and printing speed ranging between 6 and 7 mm/s.

2.3 Thermal characterization

The thermal properties of the polymer and nanocomposite were characterized using a differential scanning calorimeter (DSC, TA Instruments Q 2000). The samples of weight 3-5 mg were scanned between -70°C and 200°C at a scanning rate of 10°C min^{-1}. The samples were subjected to a heat-cool-heat cycle to remove any processing history. Thermal

degradation was performed on the samples using a thermogravimetric analyzer (TGA, TA Instruments Q 500). Samples of 3-5mg were heated from 40°C to 800°C at a heating rate of 10 °C min^{-1} under an inert atmosphere.

2.4 Shape-memory characterization

Shape memory properties of both the 3D printed polymer and composite structures were assessed by performing a shape memory testing cycle using TA instruments-Q800, Dynamic Mechanical Analysis (DMA). The samples for this test were prepared by 3D printing the materials into rectangular strips of 25×6×1 mm^3. The test was performed in stress-controlled tension mode in the following program:

i) Deformation: The printed sample was heated to a temperature T_d (deformation temperature slightly above T_g) and equilibrated for 5 min, which gives the initial strain. The sample was then stretched isothermally from 0.001 to 0.025 MPa with a stress ramp rate of 0.005 MPa/min. The strain at this point was denoted as deformed strain ($\varepsilon_{deformed}$).

ii) Cooling: The sample was then cooled to 0°C (much below T_g) at a rate of 5°C min^{-1}. It was equilibrated for 5 min under the application of constant force.

iii) Fixing: The external force was unloaded isothermally at a rate of 0.005 MPa/min. It was again equilibrated at 0°C for 5 min, and the strain captured at this point was fixed strain (ε_{fix}).

iv) Recovery: The sample was reheated at a rate of 5°C min^{-1} to T_d and equilibrated for 10 min. The recorded strain is indicated as the residual strain after recovery (ε_{recov}). The sample was finally cooled down to 0°C.

$$R_f(\%) = \frac{\varepsilon_{fix}}{\varepsilon_{deformed}} \times 100\%$$

$$R_r(\%) = \frac{\varepsilon_{deformed} - \varepsilon_{recovered}}{\varepsilon_{deformed} - \varepsilon_{initial}} \times 100\%$$

2.5 Morphological and chemical characterization

Fe_3O_4 nanoparticles were characterized for their morphology and chemical structure using a scanning electron microscope (Ultra 55 FESEM, Karl Zeiss Mono) and X-ray diffractometer (XRD), respectively. The particles were dispersed homogeneously in ethanol before drop casting over silicon wafers, which were mounted on an aluminum stub, sputter coated with gold, and then imaged under SEM. An accelerating voltage of 4 kV and a secondary electron detector (SE2) was used.

PLAMC- Fe_3O_4 composites were 3D printed into disc-shaped structures, desiccated, and gold-sputtered before visualization under SEM. PLAMC and PLAMC- Fe_3O_4 composites were characterized for chemical structure using Fourier transform infrared spectroscopy- attenuated total reflectance (FTIR-ATR) analysis on a Perkin Elmer Fourier spectrometer, USA. The spectra were recorded in the range of 650-400 cm^{-1} with a resolution of 4 cm^{-1}.

2.6 Magnetic field heating of PLMC-Fe_3O_4 nanocomposites

Magnetic hyperthermia heating was achieved by using the Ambrell Easyheat Induction system (10 kW). The magnetic field generated inside the coil was kept at ≈40 kA m^{-1} (≈500 Gauss). The magnetic field oscillated at a frequency of 215 kHz. The power delivered at the center of the hyperthermia coil was kept in the range of 3.7 kW to 4.1 kW.

2.7 *In vitro* cytocompatibility

NIH-3T3 cells were cultured in DMEM high glucose cell culture media (supplemented with 10% FBS). Sterilized samples were then seeded with fibroblast cells (NIH-3T3) at 8-10 passages at a density of 10,000 cells/cm^2. Cell growth was monitored using Alamar blue assay following the manufacturer's protocol (Thermo Fisher Scientific, USA). Cells at day 3 post seeding were also stained with Calcein-AM/ Ethidium homodimer (EtDi, EthD-1; Thermo-

fisher scientific, USA) to visually analyze the toxicity of prepared samples. Morphology of seeded cells was also analyzed on Days 3 and 5 using Phalloidin (Alexa fluor 488, Thermo Fisher Scientific, USA)/DAPI (4′,6-diamidino-2-phenylindole, Thermo Fisher Scientific, USA) double staining.

2.8 *In vivo* biocompatibility assessment

The *in vivo* toxicity of the scaffolds was assessed using Wistar rats. All the animal work was performed in accordance with 86/609/EEC act and approved by the Institute Animal Ethics Committee of the Indian Institute of Science, Bangalore (protocol number CAF/Ethics/878/2022). Adult male Wistar rats aged 8-10 months, weighing 190–230 g, were housed in well-ventilated cages supplied with autoclaved sawdust beddings. Food and sterile water were given ad libitum. 12 h light and dark cycle was maintained in the animal house at 25 ± 1 °C with 55±5% humidity. The surgeries and experiments were performed in the light cycle. The animals were divided into three groups, i.e., sham, PLMC, and composite scaffolds, with each group containing three animals. All the animals were anesthetized on day 15 by injecting a cocktail of 80 mg/kg ketamine and 15 mg/kg xylazine intraperitoneally. The coat around the mid-dorsal area of anesthetized animals was shaven and sterilized with betadine, and a horizontal incision of approximately 1.5 cm was made in the skin with a sterile surgical blade to create a subcutaneous pocket. UV sterilized scaffolds were implanted inside the subcutaneous pocket, and the incision was closed with 4.0 sutures. No implantation was done in sham control rats. At the end of 15 days, the animals were sacrificed, and the skin tissue around the implant site was excised and preserved in formalin solution (10% in PBS). Vital organs, such as the kidney and liver, were also taken out for evaluation and preserved in the formalin solution. The fixed tissue was then embedded in paraffin, and tissue sections of 5 μm were prepared by microtome. The obtained sections were stained with hematoxylin and Eosin (H&E) and imaged under a light microscope (IX-53, Olympus).

To assess any inflammatory response, hematological parameters were also checked. On day 7 and day 15, 1 ml of blood was collected from each animal. The blood was collected in heparin-coated tubes for the estimation of Total Leukocyte Count (TLC), Erythrocyte Sedimentation Rate (ESR), Serum glutamic pyruvic transaminase (SGPT) and Serum Glutamic-Oxaloacetic Transaminase (SGOT).

2.9 Statistical analysis

The results are presented as mean ± standard error for each group. GraphPad Prism 5.04 was used for the statistical analysis (GraphPad Software, San Diego, CA, USA). One-way ANOVA was used for the statistical analysis, which was then followed by Dunnett and Tukey tests for significance. All analyses were carried out at a 95% confidence level and were significant at statistical probability (p-value) <0.05. Statistical significances were denoted as (*), (**) and (***) for $p < 0.05$, $p < 0.01$ and $p < 0.001$, respectively.

3. Results and discussion

PLMC typically exhibits glass transition in the broad range of 20°C to 45°C, depending on its molecular weight, monomer (lactide(L): trimethylene carbonate(TMC)) ratio[28], etc. The ratio of L:TMC was 70:30 in the copolymer used in this study. PLMC-Fe_3O_4 composites containing 2.5%, 5%, and 10% (by weight) Fe_3O_4 nanoparticles (diameter in the range of 50-100 nm) were prepared by solvent casting. 10% composites were difficult to print because of frequent clogging of the nozzles during printing owing to high melt viscosity. 2.5% composite structures exhibited minimal shape recoveries under magnetic field, as the particle content was low. Hence, 5% content was determined to be optimal as it was easily processable by printing and exhibited good shape recoveries. Only the 5% composite was used for further studies.

As seen from figure 2a, DSC thermograms reveal the T_g of PLMC to be ≈33°C, whereas that of the PLMC-Fe_3O_4(5%) composite is marginally lower (by 3°) at 30°C. This change is attributed to the plasticizing effect of the nanoparticles, which reduces the thermal energy required for the segmental motions of the polymer chains[29]. Both the PLMC and nanocomposites also exhibit cold crystallization at ≈112°C and ≈95°C, respectively, due to the formation of crystals from the quenched-in amorphous structure above T_g[30]. Melting of PLMC occurs at 154°C, whereas the composite at 158°C, which is due to increased melt viscosity of the composite in the presence of nanoparticles. While some studies report PLMC to be amorphous[28], other studies indicate its semi-crystalline nature[31]. Hence, the crystallinity depends on the molecular weight, polymerization kinetics, etc. The PLMC used in this study did exhibit sharp melting peaks in the DSC analysis.

Figure 2b reveals the tan δ values of PLMC and its composite, as recorded from temperature sweeps performed by DMA (dynamic mechanical analysis). T_g calculated from the peak of tan δ of PLMC is 53°C, whereas it is 51°C for the composite. It is to be noted that DSC captures the thermal transitions in a polymer alone, without accounting for mechanical forces which might influence the T_g values. In contrast, DMA is a more sensitive technique that captures the mechanical vibrations inside the polymer chains along with the thermal transitions, thereby resulting in different and higher T_g values than from DSC[32]. Also, the polymer specimen remains stretched in DMA, whereas DSC measures the T_g of unstretched samples[33].

The TGA (thermogravimetric analysis) results indicate that thermal degradation of PLMC starts at ≈240°C while the composite starts to degrade at ≈285°C, as observed in figure 2c. These data aid in determining the optimal printing temperatures and times to minimize thermal degradation of the materials during melt extrusion-based 3D printing. TGA also confirmed the nanofiller content in the polymer matrix to be ≈5%. As observed in figure 2d, the DTG

(derivative thermogravimetric analysis) curves show the temperature of maximum decomposition rate for PLMC to be 300°C and composite to be 310°C.

Figure S1 confirms the structure of iron oxide nanoparticles from XRD and morphology from SEM. FTIR results in Figure S2 show the absence of any new chemical bond formation following the incorporation of nanoparticles in the PLMC matrix. This lack of interaction is due to the absence of functionalization in the particles, which only allows physical interaction with the polymer matrix. The peaks at 1085, 1187, and 1746 cm^{-1} correspond to C-O stretching, C-C stretching, and –C=O vibration, respectively, in both neat PLMC and the composite samples corroborating the data from other studies on PLMC reported in the literature[16]. SEM images of the 3D printed composite structures confirm the excellent printability by extrusion printing technique.

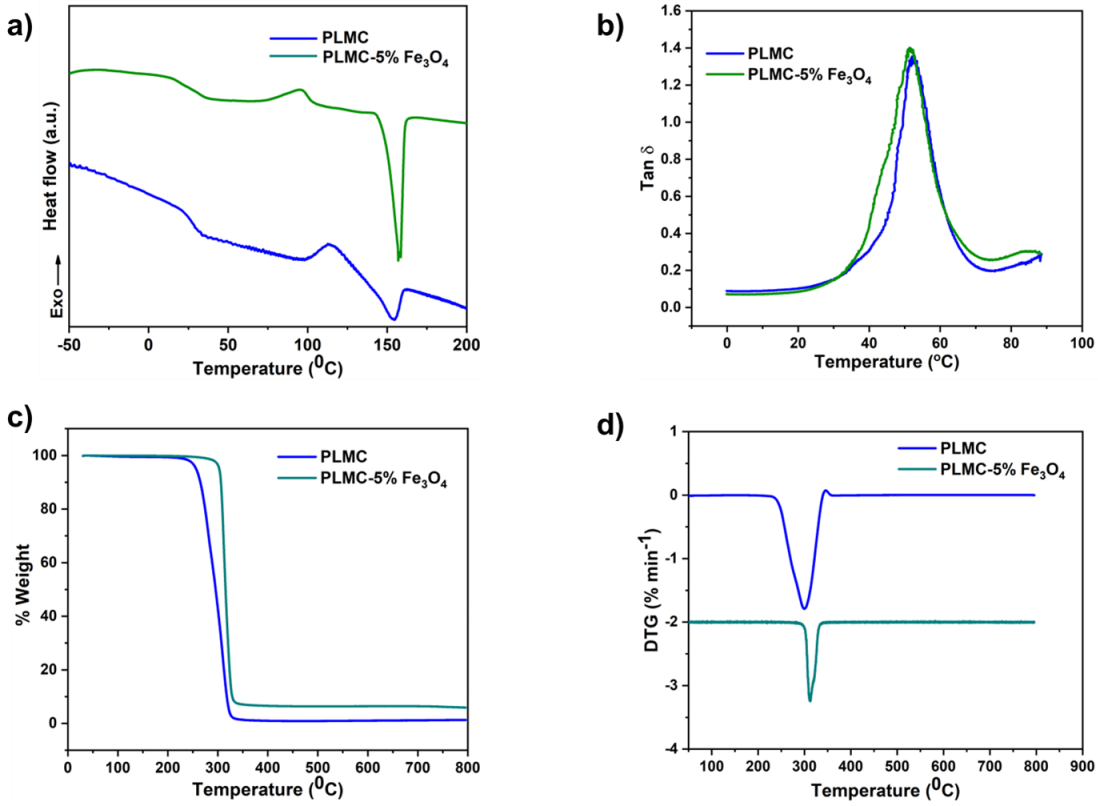

Figure 2: Thermal and dynamic thermo-mechanical characterizations of PLMC and its composite. a) DSC thermograms, b) tan δ (damping factor) as a function of temperature, c) TGA curves, and d) DTG curves versus temperature.

Figure 3 compiles the shape memory characteristics of neat PLMC and its magnetic nanocomposite. As calculated from the shape memory testing routines, PLMC exhibited excellent shape fixing of ≈95% and shape recovery of ≈99%. Similarly, the PLMC-Fe_3O_4 composite exhibited ≈97% shape fixing and ≈99% shape recovery. The slightly enhanced shape fixing in the composite could be due to increased resistance in polymer chain motions offered by the stiff nanofillers below T_g. It is to be noted that shape recovery of PLMC starts at 44°C and composite at 41°C, as indicated by shape recovery onset temperature (T_s) in figure 3 (b and d). T_s can differ from T_g and indicates the temperature at which macroscopic shape recovery occurs. It can also be observed from figure S3 that the storage modulus exhibits a sharp drop with an increase in temperature. Cyclic thermomechanical testing was also performed for both the materials for up to three cycles, as shown in figure S3. It is observed that PLMC sustained good fixing and recovery ratios, except for the first cycle[34]. The composite displayed excellent shape fixing and recovery ratios for the first cycle with a reduction in the properties in the subsequent cycles. It is known that the cyclic shape memory performance is highly dependent on testing parameters such as deformation rate, fixing temperature, recovery time, etc[35]. Hence, these results may vary with different testing conditions.

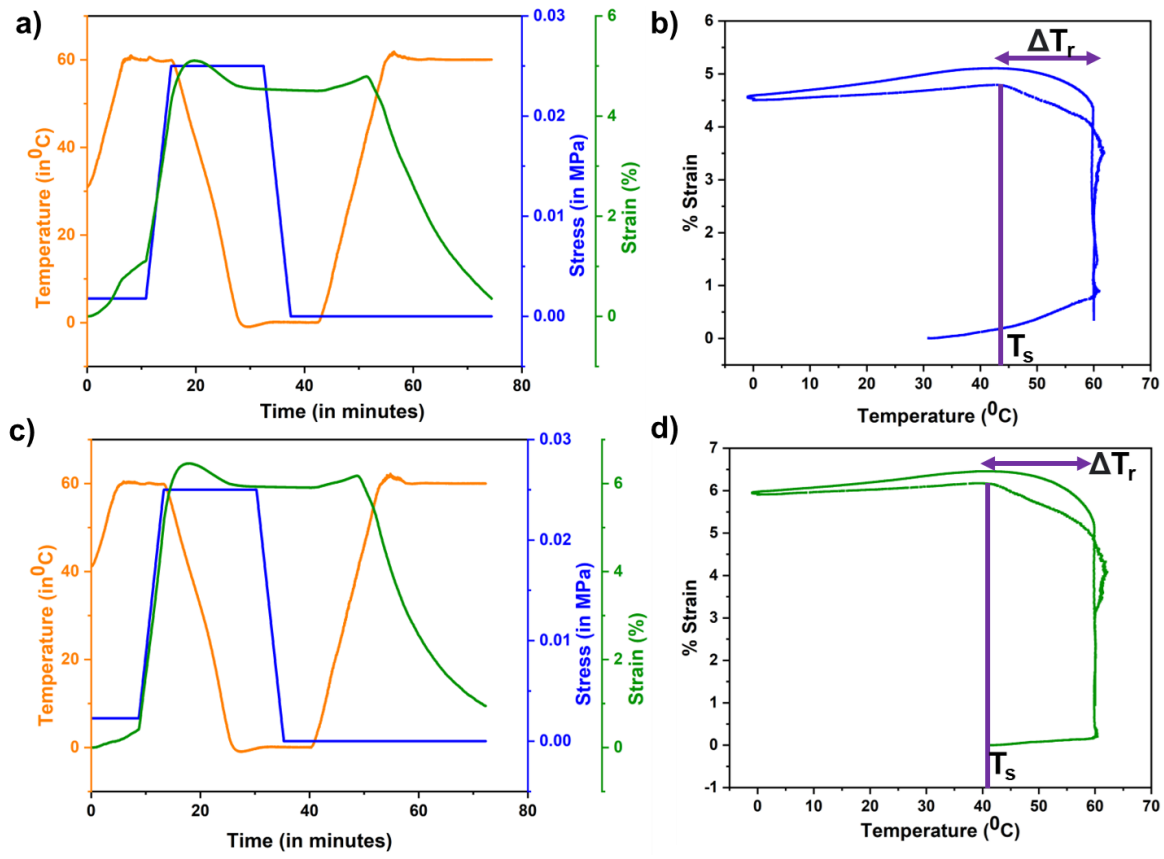

Figure 3: Shape memory characterization of PLMC and its composite. a) Thermomechanical shape memory testing of PLMC, b) strain profile of PLMC with temperature, c) Thermomechanical shape memory testing of PLMC composite, d) strain profile of PLMC composite with temperature.

Next, PLMC-5% Fe_3O_4 composites were 3D printed into planar (2D) shapes and fixed into temporary shapes below T_g. Upon placing them in an alternating magnetic field, they recovered back to their original shapes by inductive heating, as shown in figure S4. It is due to the fact that Fe_3O_4 nanoparticles act as localized heating sources inside the composite, and once the temperature reaches sufficiently above T_g, the composite macroscopically changes its shape to recover to its initial confirmation. The extent of recovery was around 95% for all the shapes, and recovery time was 45 to 60 s.

3D constructs of these composites were also printed wherein specific infill patterns (rectilinear) and densities (30%) were used to lay down material, as these infill parameters are most common in literature. The printed 3D constructs were fixed at 0°C and then were able to recover to their original shapes on magnetic actuation. In contrast to 2D shapes, 3D constructs were able to recover much faster (under 15 s) and better (>99%), as shown in figure 4 and supplementary videos V4, V5 and V6. This is because of a higher amount of material which corresponds to a higher number of heating elements and a higher specific absorption rate (SAR)[36]. SAR is defined as the rate of thermal energy dissipated by a material under an alternating magnetic field[37].

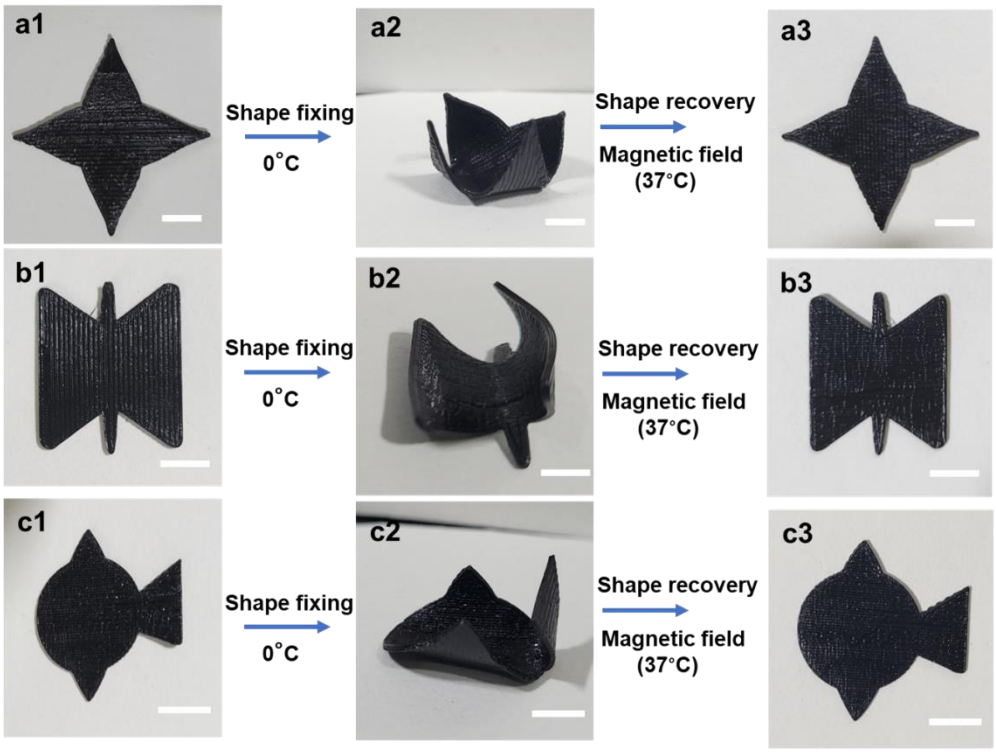

Figure 4: Shape recovery of 3D printed PLMC-5% Fe_3O_4 (3D structures) under alternating magnetic field; a1) As printed petal shape, a2) Deformed and fixed ($<T_g$) petal, a3) Recovered ($>T_g$) petal, b1) As printed butterfly shape, b2) Deformed and fixed ($<T_g$) butterfly, b3) Recovered ($>T_g$) butterfly, c1) As-printed fish shape, c2) Deformed and fixed ($<T_g$) fish, c3) Recovered ($<T_g$) fish (Scale bar is 10 mm)

The particle size, concentration, and distribution of nanofillers in SMP directly impact the recovery performance and time[38]. Different studies report a minimum of 10 to 15 wt% of Fe_3O_4 nanoparticles in the SMP matrix to trigger sufficient inductive heating and shape recovery[39]. However, in this study, only 5 wt% concentration of nanoparticles was sufficient to realize shape recovery in the SMP by the magnetic field. This is highly advantageous because of better dispersions, reduced agglomeration, and ease of processability. Moreover, a higher loading of nanoparticles may adversely affect cell viability.[40]

For *in vivo* applications, direct heating is not feasible owing to the poor thermal conductivity of polymers which then warrants the surrounding regions to be heated high enough to trigger shape recovery. Moreover, the tissues deep inside are not accessible to trigger shape recovery through contact heating. Magnetic composites offer a potential benefit allowing for a contactless recovery through inductive heating, which is very localized and doesn't require heating of the neighboring tissues. Figure 5a shows 3D printed composite scaffolds (printed using a 30% rectilinear infill pattern), which in their original disc confirmation, are not deployable. They could be easily deformed and fixed into flattened discs, which could now be delivered inside a tube. The scaffolds showed excellent shape recovery (>99%) under 15 s inside a magnetic field, as shown in video V7. The corresponding thermal images in figure S5 show the maximum temperature at the core of the scaffold is 40°C after complete recovery. In another case, the composites printed and fixed into tubular shapes could recover when constricted inside a glass tube within 10 s, as shown in figure 5b and video V8. This proof-of-concept demonstrates the potential of exploiting such materials as self-fitting scaffolds for various tissues. Apart from offering a benign actuation strategy, magnetic composites can also be remotely guided by permanent magnets to the site of deployment, as shown in video V8.

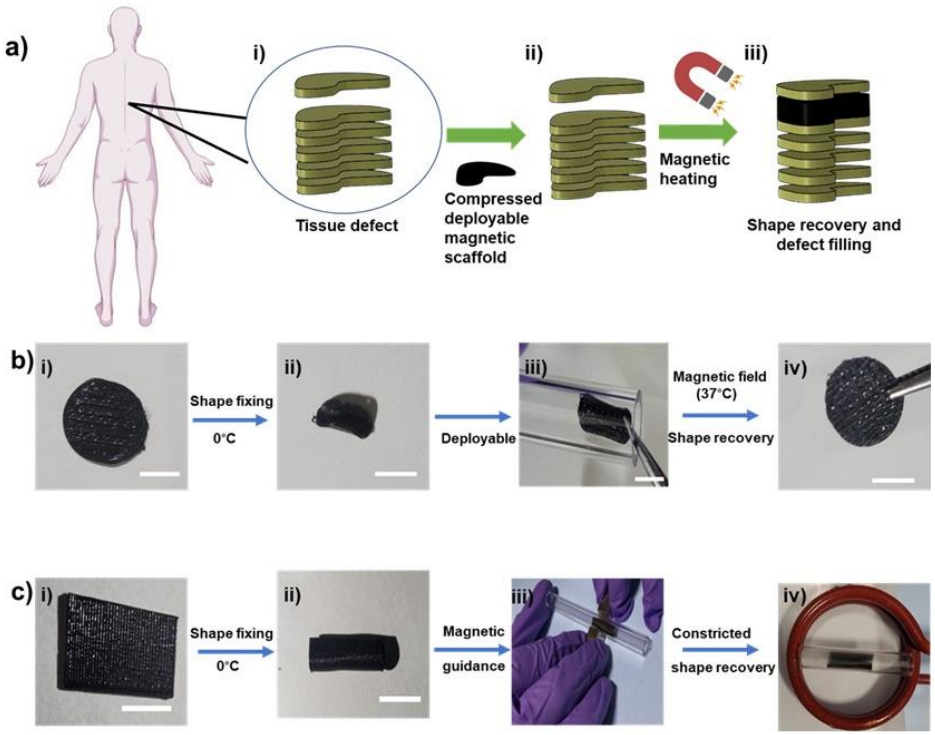

Figure 5: a) Schematic highlighting deployable tissue scaffolds. i) Tissue defect inside the human body, ii) 3D printed composite scaffold compressed and deployed in a minimally-invasive manner, iii) Inductive heating to trigger shape recovery of the magnetic scaffold and confirm to defect shape; b) Shape recovery of 3D printed PLMC-5% Fe_3O_4 composites as deployable tissue scaffolds under alternating magnetic field. i) As-printed disc-shaped scaffold, ii) Scaffold is not able to pass through a tube in original conformation, iii) Deformed and fixed scaffold ($<T_g$), iv) Fixed scaffold able to be deployed through tube ($>T_g$), v) Recovered scaffold (Scale bar is 5 mm); b) Restrictive shape recovery of pre-programmed shape to original shape; c) As-printed PLMC-5% Fe_3O_4 composite, ii) Deformed and fixed shape, iii) Magnetically guided and recovery of pre-programmed structure into original shape under alternating magnetic field. (Scale bar is 10 mm)

Next, neat PLMC and PLMC magnetic composites were used to print specific parts inside a single structure, as shown in figure 6. The structures were deformed and fixed into pre-programmed shapes below the T_g. The portions printed with the composite only recovered inside an alternating magnetic field, as neat PLMC is not magnetically responsive (as shown in videos V9-V12 for a variety of structures). The partially recovered structures are stable unless a direct heating stimulus is provided when PLMC parts also begin to recover yielding completely recovered structures. This offers sequential and selective stimulation of parts in a structure. Such concepts could find use in soft robotics[41-42], grippers[43-44], etc., wherein distinct regions of a macro-structure need to be actuated at one time.

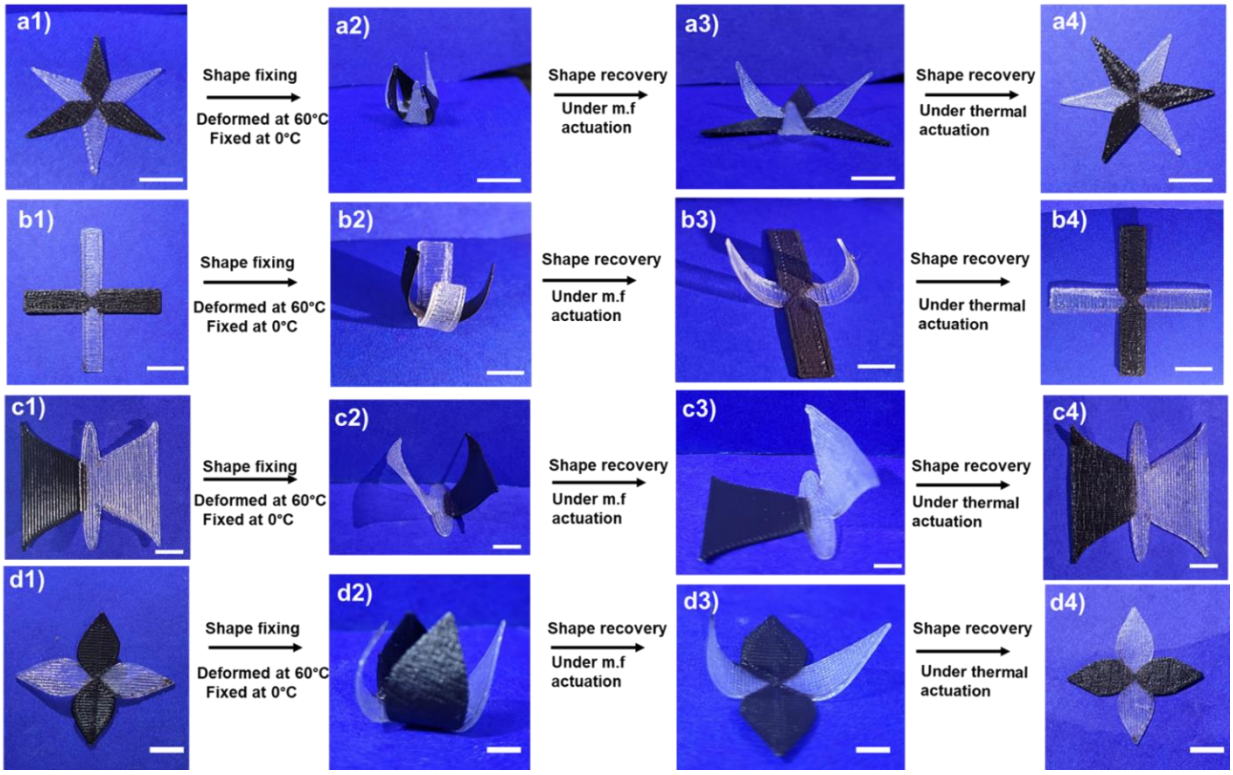

Figure 6: Shape recovery of 3D printed PLMC and PLMC-5% Fe_3O_4 composite dual structures sequentially and selectively actuated under alternating magnetic field and then heat; a1) Dual-printed star, a2) Deformed star, a3) Partially recovered star by indirect heating, a4) Fully recovered star by direct heating, b1) Dual-printed cross, b2) Deformed cross, b3) Partially recovered cross by indirect heating, b4) Fully recovered cross by direct heating, c1)

Dual-printed butterfly, c2) Deformed butterfly, c3) Partially recovered butterfly by indirect heating, c4) Fully recovered butterfly by direct heating, d1) Dual-printed petal, d2) Deformed petal, d3) Partially recovered petal by indirect heating, d4) Fully recovered petal by direct heating (Scale bar is 10 mm)

Next, the in vitro biocompatibility of the materials was assessed using NIH 3T3 cells. The results of cytocompatibility analysis are compiled in figure 7. Live/dead staining (figure 7a) demonstrated that both PLMC and composite did not show any toxicity to the cultured cells. Most of the cells were viable with very minimal cell death. Also, the cells adhered and proliferated in number over time on both the materials, as seen from the Alamar blue assay (figure 7b), indicating excellent biocompatibility. Further, cytoskeletal staining on different days (figure 7c) demonstrates that cells could adhere and spread on the surface of the materials.

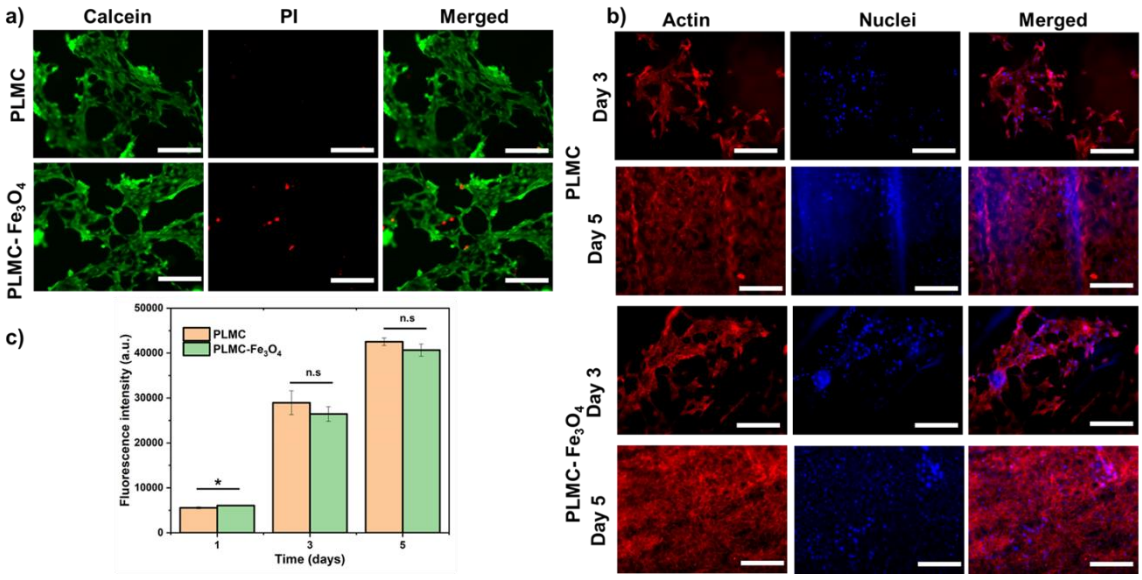

Figure 7: *In vitro* biological characterization of PLMC and its composite. a) Live-dead assay, b) Cytoskeletal staining, and c) Alamar blue assay. * denotes $p<0.05$, n.s is non-significant. (Scale bar is 100 µm)

Since this nanocomposite has great potential to be extended for biomedical applications, *in vivo* biocompatibility was also assessed in Wistar rats. The results of *in vivo* biocompatibility are compiled in figure 8. Histological observations on different days post-implantation (Days 7 and 14) demonstrated that both PLMC and the nanocomposite did not elicit any major inflammatory tissue response at the site of implantation. The surrounding skin displayed healthy physiology with loosely packed extracellular matrix (ECM), skin appendages, and the absence of infiltrating inflammatory cells. Further, to confirm the inflammatory response from scaffold remnants and/or degraded products, histological observations of two vital organs, the liver and kidney, were also observed. As seen in Figure 7, healthy physiology of both organs was observed with no signs of inflammation. Normal lobular morphology of the liver and the characteristic kidney morphology with intact glomerulus and glomerular-capsular space in Sham, PLMC, and composite groups. Further, normal blood parameters in all groups confirmed the absence of any cytotoxicity induced by the implanted polymers (figure S6).

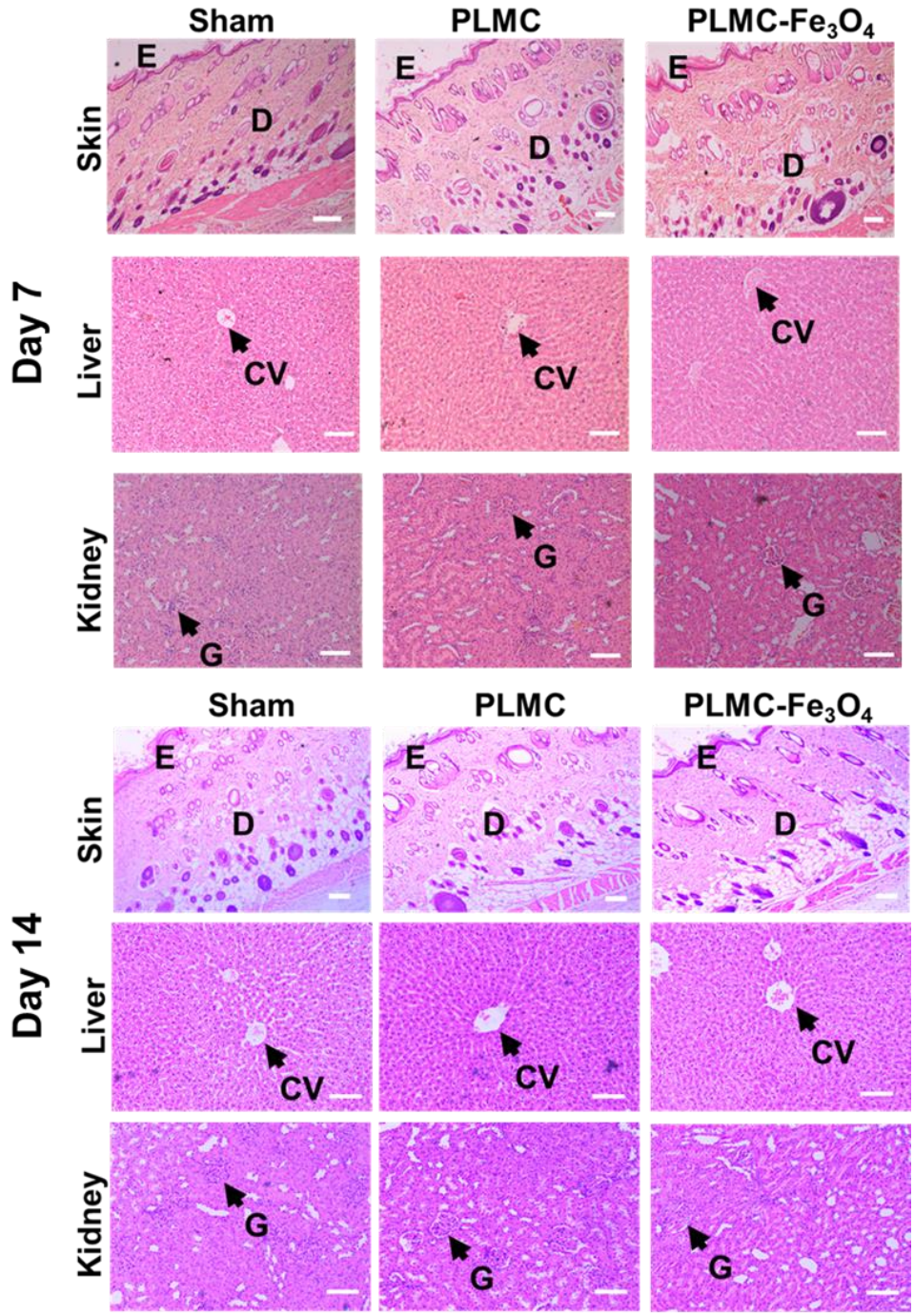

Figure 8: *In vivo* biological characterization of PLMC and composites. Histological staining of skin, liver, and kidney sections in Sham, PLMC, and nanocomposite groups on day 7 and day 14 (scale bar is 100 µm for all images except for skin tissues, where the scale bar is 200 µm).

The distinct advantages of our material system are excellent shape recoveries (>99%), and extremely fast (under 15 s for 3D structures) at physiological temperatures (≈37°C), which are ideal for biomedical applications. Extrusion-based printing was used, which is advantageous over other strategies like direct ink writing, which involve toxic solvents and post-processing steps. Also, the concentration of Fe_3O_4 nanofillers used is very low (i.e., 5% w/w) compared to other studies, which report at least 15% (w/w). Lower filler concentrations are always advantageous because of easy processability and lower risks of associated nanotoxicities[45]. The magnetic composites were printed into 3D porous scaffolds that could be potentially deployed to the site of tissue defects and triggered through inductive heating to conform to the defect size. *In vitro* and *in vivo* biocompatibility of PLMC and its composites were assessed to highlight the importance of the material systems as deployable tissue scaffolds. Additionally, PLMC and PLMC- Fe_3O_4 composites were printed selectively in different regions of the same structure to have sequential and selective stimulation under heating and magnetic field actuation, respectively.

Conclusion

In this study, novel PLMC- 5% Fe_3O_4 composites were 3D printed via extrusion-based printing. The printed composites exhibited excellent shape fixity ratios (≈95%) and shape recovery ratios (≈99%) for both 2D and 3D shapes. The key advantages were short recovery times (under 15 s) at physiologically relevant recovery temperatures (≈40°C). The composites were also printed into porous tissue scaffolds. The scaffolds were compressed into shapes that can be deployable in a minimally invasive manner, magnetically guided, and were recovered (≈99%)) by inductive heating to original shapes. The composites showed favorable *in vitro* and *in vivo* biocompatibility. These features make it highly conducive for being employed as self-fitting scaffolds and other biomedical applications. Neat PLMC and PLMC composites were used to print distinct regions in a single structure, which then exhibited selective and sequential

recovery through direct and inductive heating. Taken together, PLMC-based magnetic nanocomposites pave the way for a multitude of applications spanning robotics, advanced manufacturing, biomedical areas, etc. that demand excellent and fast shape recoveries with complex geometries.

Acknowledgements

The authors thank the Department of Science and Technology (DST) (DST/NM/NB/2018/119(G)) and the Science and Engineering Research Board (SERB) (IPA/2020/000025) for the financial support. We acknowledge Dr. Suhela Tyeb for her help in animal studies. We thank Central Animal Facility (CAF) for extending the facilities for animal studies. S.C. acknowledges support from the Prime Minister's Research Fellowship. A.J. acknowledges IoE fellowship from IISc.

References:

1. Panda, B.; Paul, S. C.; Hui, L. J.; Tay, Y. W. D.; Tan, M. J., Additive manufacturing of geopolymer for sustainable built environment. *Journal of Cleaner Production* **2017,** *167*, 281-288.
2. Bhatt, P. M.; Malhan, R. K.; Shembekar, A. V.; Yoon, Y. J.; Gupta, S. K., Expanding capabilities of additive manufacturing through use of robotics technologies: A survey. *Additive Manufacturing* **2020,** *31*, 100933.
3. Ramola, M.; Yadav, V.; Jain, R., On the adoption of additive manufacturing in healthcare: a literature review. *Journal of Manufacturing Technology Management* **2018**.
4. Choi, J.; Kwon, O.-C.; Jo, W.; Lee, H. J.; Moon, M.-W., 4D printing technology: a review. *3D Printing and Additive Manufacturing* **2015,** *2* (4), 159-167.
5. Scalet, G. In *Two-way and multiple-way shape memory polymers for soft robotics: An overview*, Actuators, Multidisciplinary Digital Publishing Institute: 2020; p 10.
6. Ze, Q.; Kuang, X.; Wu, S.; Wong, J.; Montgomery, S. M.; Zhang, R.; Kovitz, J. M.; Yang, F.; Qi, H. J.; Zhao, R., Magnetic shape memory polymers with integrated multifunctional shape manipulation. *Advanced Materials* **2020,** *32* (4), 1906657.
7. Santo, L.; Quadrini, F.; Accettura, A.; Villadei, W., Shape memory composites for self-deployable structures in aerospace applications. *Procedia Engineering* **2014,** *88*, 42-47.
8. Delaey, J.; Dubruel, P.; Van Vlierberghe, S., Shape-memory polymers for biomedical applications. *Advanced Functional Materials* **2020,** *30* (44), 1909047.

9. Sun, L.; Huang, W.; Wang, C.; Zhao, Y.; Ding, Z.; Purnawali, H., Optimization of the shape memory effect in shape memory polymers. *Journal of Polymer Science Part A: Polymer Chemistry* **2011,** *49* (16), 3574-3581.
10. Yang, X.; Wang, L.; Wang, W.; Chen, H.; Yang, G.; Zhou, S., Triple shape memory effect of star-shaped polyurethane. *ACS Applied Materials & Interfaces* **2014,** *6* (9), 6545-6554.
11. Wu, Y.; Hu, J.; Zhang, C.; Han, J.; Wang, Y.; Kumar, B., A facile approach to fabricate a UV/heat dual-responsive triple shape memory polymer. *Journal of Materials Chemistry A* **2015,** *3* (1), 97-100.
12. Yakacki, C. M.; Shandas, R.; Lanning, C.; Rech, B.; Eckstein, A.; Gall, K., Unconstrained recovery characterization of shape-memory polymer networks for cardiovascular applications. *Biomaterials* **2007,** *28* (14), 2255-2263.
13. Huang, W. M.; Song, C. L.; Fu, Y. Q.; Wang, C. C.; Zhao, Y.; Purnawali, H.; Lu, H. B.; Tang, C.; Ding, Z.; Zhang, J. L., Shaping tissue with shape memory materials. *Advanced Drug Delivery Reviews* **2013,** *65* (4), 515-535.
14. Small Iv, W.; Wilson, T. S.; Benett, W. J.; Loge, J. M.; Maitland, D. J., Laser-activated shape memory polymer intravascular thrombectomy device. *Optics Express* **2005,** *13* (20), 8204-8213.
15. Hu, J.-J.; Lei, Q.; Zhang, X.-Z., Recent advances in photonanomedicines for enhanced cancer photodynamic therapy. *Progress in Materials Science* **2020,** *114*, 100685.
16. Wan, X.; Wei, H.; Zhang, F.; Liu, Y.; Leng, J., 3D printing of shape memory poly (d, l-lactide-co-trimethylene carbonate) by direct ink writing for shape-changing structures. *Journal of Applied Polymer Science* **2019,** *136* (44), 48177.
17. Dai, S.; Yue, S.; Ning, Z.; Jiang, N.; Gan, Z., Polydopamine Nanoparticle-Reinforced Near-Infrared Light-Triggered Shape Memory Polycaprolactone–Polydopamine Polyurethane for Biomedical Implant Applications. *ACS Applied Materials & Interfaces* **2022,** *14* (12), 14668-14676.
18. Li, G.; Yan, Q.; Xia, H.; Zhao, Y., Therapeutic-Ultrasound-Triggered Shape Memory of a Melamine-Enhanced Poly(vinyl alcohol) Physical Hydrogel. *ACS Applied Materials & Interfaces* **2015,** *7* (22), 12067-12073.
19. Liu, W.; Wang, A.; Yang, R.; Wu, H.; Shao, S.; Chen, J.; Ma, Y.; Li, Z.; Wang, Y.; He, X., Water-triggered stiffening of shape memory polyurethanes composed of hard backbone dangling PEG soft segments. *Advanced Materials* **2022**, 2201914.
20. Yu, K.; Liu, Y.; Leng, J., Shape memory polymer/CNT composites and their microwave induced shape memory behaviors. *Rsc Advances* **2014,** *4* (6), 2961-2968.
21. Soto, G. D.; Meiorin, C.; Actis, D. G.; Mendoza Zélis, P.; Moscoso Londoño, O.; Muraca, D.; Mosiewicki, M. A.; Marcovich, N. E., Magnetic nanocomposites based on shape memory polyurethanes. *European Polymer Journal* **2018,** *109*, 8-15.
22. Gu, S.-Y.; Chang, K.; Jin, S.-P., A dual-induced self-expandable stent based on biodegradable shape memory polyurethane nanocomposites (PCLAU/Fe3O4) triggered around body temperature. *Journal of Applied Polymer Science* **2018,** *135* (3), 45686.
23. Mohr, R.; Kratz, K.; Weigel, T.; Lucka-Gabor, M.; Moneke, M.; Lendlein, A., Initiation of shape-memory effect by inductive heating of magnetic nanoparticles in thermoplastic polymers. *Proceedings of the National Academy of Sciences* **2006,** *103* (10), 3540-3545.

24. Wei, H.; Zhang, Q.; Yao, Y.; Liu, L.; Liu, Y.; Leng, J., Direct-write fabrication of 4D active shape-changing structures based on a shape memory polymer and its nanocomposite. *ACS applied materials & interfaces* **2017,** *9* (1), 876-883.
25. Zhao, W.; Zhang, F.; Leng, J.; Liu, Y., Personalized 4D printing of bioinspired tracheal scaffold concept based on magnetic stimulated shape memory composites. *Composites Science and Technology* **2019,** *184*, 107866.
26. Zhang, F.; Wang, L.; Zheng, Z.; Liu, Y.; Leng, J., Magnetic programming of 4D printed shape memory composite structures. Elsevier: 2019.
27. Wan, X.; He, Y.; Liu, Y.; Leng, J., 4D printing of multiple shape memory polymer and nanocomposites with biocompatible, programmable and selectively actuated properties. *Additive Manufacturing* **2022,** *53*, 102689.
28. Bao, M.; Lou, X.; Zhou, Q.; Dong, W.; Yuan, H.; Zhang, Y., Electrospun biomimetic fibrous scaffold from shape memory polymer of PDLLA-co-TMC for bone tissue engineering. *ACS applied materials & interfaces* **2014,** *6* (4), 2611-2621.
29. Zheng, X.; Zhou, S.; Xiao, Y.; Yu, X.; Li, X.; Wu, P., Shape memory effect of poly (d, l-lactide)/Fe3O4 nanocomposites by inductive heating of magnetite particles. *Colloids and Surfaces B: Biointerfaces* **2009,** *71* (1), 67-72.
30. Righetti, M. C., Crystallization of polymers investigated by temperature-modulated DSC. *Materials* **2017,** *10* (4), 442.
31. Fuoco, T.; Mathisen, T. r.; Finne-Wistrand, A., Poly (l-lactide) and poly (l-lactide-co-trimethylene carbonate) melt-spun fibers: structure–processing–properties relationship. *Biomacromolecules* **2019,** *20* (3), 1346-1361.
32. Ferrillo, R. G.; Achorn, P. J., Comparison of thermal techniques for glass transition assignment. II. Commercial polymers. *Journal of Applied Polymer Science* **1997,** *64* (1), 191-195.
33. Sharifi, S.; van Kooten, T. G.; Kranenburg, H.-J. C.; Meij, B. P.; Behl, M.; Lendlein, A.; Grijpma, D. W., An annulus fibrosus closure device based on a biodegradable shape-memory polymer network. *Biomaterials* **2013,** *34* (33), 8105-8113.
34. Sauter, T.; Heuchel, M.; Kratz, K.; Lendlein, A., Quantifying the Shape-Memory Effect of Polymers by Cyclic Thermomechanical Tests. *Polymer Reviews* **2013,** *53* (1), 6-40.
35. Hu, J. L.; Ji, F. L.; Wong, Y. W., Dependency of the shape memory properties of a polyurethane upon thermomechanical cyclic conditions. *Polymer International* **2005,** *54* (3), 600-605.
36. Weigel, T.; Mohr, R.; Lendlein, A., Investigation of parameters to achieve temperatures required to initiate the shape-memory effect of magnetic nanocomposites by inductive heating. *Smart Materials and Structures* **2009,** *18* (2), 025011.
37. Evans, B. A.; Bausch, M. D.; Sienerth, K. D.; Davern, M. J., Non-monotonicity in the influence of nanoparticle concentration on SAR in magnetic nanoparticle hyperthermia. *Journal of Magnetism and Magnetic Materials* **2018,** *465*, 559-565.
38. Ma, M.; Wu, Y.; Zhou, J.; Sun, Y.; Zhang, Y.; Gu, N., Size dependence of specific power absorption of Fe3O4 particles in AC magnetic field. *Journal of Magnetism and Magnetic Materials* **2004,** *268* (1), 33-39.
39. Salkhi Khasraghi, S.; Shojaei, A.; Janmaleki, M.; Sundararaj, U., Efficient inductively heated shape memory polyurethane acrylate network with silane modified

nanodiamond@Fe3O4 superparamagnetic nanohybrid. *European Polymer Journal* **2021,** *159*, 110735.

40. Ghasempour, S.; Shokrgozar, M. A.; Ghasempour, R.; Alipour, M., Investigating the cytotoxicity of iron oxide nanoparticles in in vivo and in vitro studies. *Experimental and Toxicologic Pathology* **2015,** *67* (10), 509-515.
41. Han, M.-W.; Ahn, S.-H., Blooming Knit Flowers: Loop-Linked Soft Morphing Structures for Soft Robotics. *Advanced Materials* **2017,** *29* (13), 1606580.
42. Jin, B.; Song, H.; Jiang, R.; Song, J.; Zhao, Q.; Xie, T., Programming a crystalline shape memory polymer network with thermo- and photo-reversible bonds toward a single-component soft robot. *Science Advances* **2018,** *4* (1), eaao3865.
43. Diller, E.; Sitti, M., Three-Dimensional Programmable Assembly by Untethered Magnetic Robotic Micro-Grippers. *Advanced Functional Materials* **2014,** *24* (28), 4397-4404.
44. Abdullah, A. M.; Li, X.; Braun, P. V.; Rogers, J. A.; Hsia, K. J., Self-Folded Gripper-Like Architectures from Stimuli-Responsive Bilayers. *Advanced Materials* **2018,** *30* (31), 1801669.
45. Soenen, S. J. H.; Nuytten, N.; De Meyer, S. F.; De Smedt, S. C.; De Cuyper, M., High Intracellular Iron Oxide Nanoparticle Concentrations Affect Cellular Cytoskeleton and Focal Adhesion Kinase-Mediated Signaling. *Small* **2010,** *6* (7), 832-842.